1.4

Reprinted from Preprint Volume: Nineteenth Conference on Radar Meteorology, April 15-18, 1980, Miami, Fla. Published by the American Meteorological Society, Boston, Mass.

AIR MOTIONS AND WATER BUDGET OF A WARM FRONTAL RAINBAND

Robert A. Houze, Jr., Steven A. Rutledge, Thomas J. Matejka and Peter V. Hobbs

Department of Atmospheric Sciences
University of Washington
Seattle, Washington 98195

1. INTRODUCTION

The organization of the clouds and precipitation in extratropical cyclones is typically dominated by mesoscale rainbands. Houze et al. (1976a) classified these rainbands according to their location within the pattern of fronts associated with a cyclone. Using data from aircraft penetrations, Matejka et al. (1980) have distinguished the microphysical properties of the clouds associated with each type of rainband and showed their relationship to substructures in the temperature patterns of the frontal baroclinic zones. Cold frontal rainbands have been described by Hobbs et al. (1980) and Herzegh and Hobbs (1980) have examined rainbands in the warm frontal regions of cyclones. The present paper is a further examination of warm frontal rainbands. Our study is based on a well-defined warm frontal rainband observed in an occluded frontal system that moved into Washington during the CYCLES (Cyclonic Extratropical Storms) PROJECT on 13 December 1977. This rainband had an orientation from northwest to southeast and moved from the southwest at 28-32 m s^{-1}. Warm frontal rainbands typically occur in the leading portions of the cloud patterns of occluded cyclones moving into the Pacific Northwest and they usually have this orientation and motion.

In general, warm frontal rainbands may be described as mesoscale features within which the widespread precipitation associated with the warm advection and general upward motion in the warm frontal region of a cyclone is enhanced. The reason for the enhancement of the precipitation is not fully understood. Observational studies have indicated that precipitation growth in warm frontal rainbands proceeds as shallow convective cells aloft generate seed crystals, which fall into thick stratiform "feeder" clouds below, where they undergo further growth before reaching the surface as precipitation. Houze et al. (1976b) and Hobbs and Locatelli (1978) have shown that, in this situation, precipitation particles undergo most of their growth below the layer containing the cells. Herzegh and Hobbs (1980), using observed vertical profiles of radar reflectivity, have quantified this result, showing that 80% of the growth of precipitation particles that were generated in cells aloft and that fell within warm frontal rainbands occurred by further deposition and aggregation below the level of the cells, within a thick stratiform cloud located mainly above the 0°C level. They also described a warm frontal rainband whose feeder cloud was located entirely below the 0°C level. For this warm feeder cloud, they again concluded that particles initiated in cells aloft fell into the feeder cloud and grew by accretion of cloud water.

These results indicate that the shallow convective cells aloft do not greatly increase the total water content of the clouds associated with a warm frontal rainband. Rather, most of the mass of the precipitation particles is acquired at low levels. Ice particles from the cells aloft, however, aid the microphysical conversion of water condensed at lower levels to precipitation, while the condensation of water vapor in the lower level cloud provides the mass of water accrued by the falling ice particles.

Herzegh and Hobbs (1980) found a mesoscale region of enhanced lifting in the lower cloud layer associated with their warm-feeder rainband. This result suggest that mesoscale lifting at low levels was dynamically enhancing the condensation of water vapor.

It appears, therefore, that the enhancement of the precipitation in warm frontal rainbands may be due to: (1) the generation of seed crystals aloft, which, as they fallout, enhance the microphysical conversion of water condensed at lower levels, or (2) dynamical enhancement of the condensation of water vapor at low levels (to increase the mass of condensate available for precipitation or (3) a combination of both of these mechanisms.

In the warm frontal rainband of the present study, we find that pronounced mesoscale lifting, similar to but stronger than that noted by Herzegh and Hobbs (1980), occurred at low levels. The Doppler radar data available for this case allow us to test quantitatively, through an examination of the air motion and water budget of the warm frontal rainband to what extent a mesoscale zone of lifting at low levels can supply through process (2) the moisture required to explain the precipitation in the rainband.

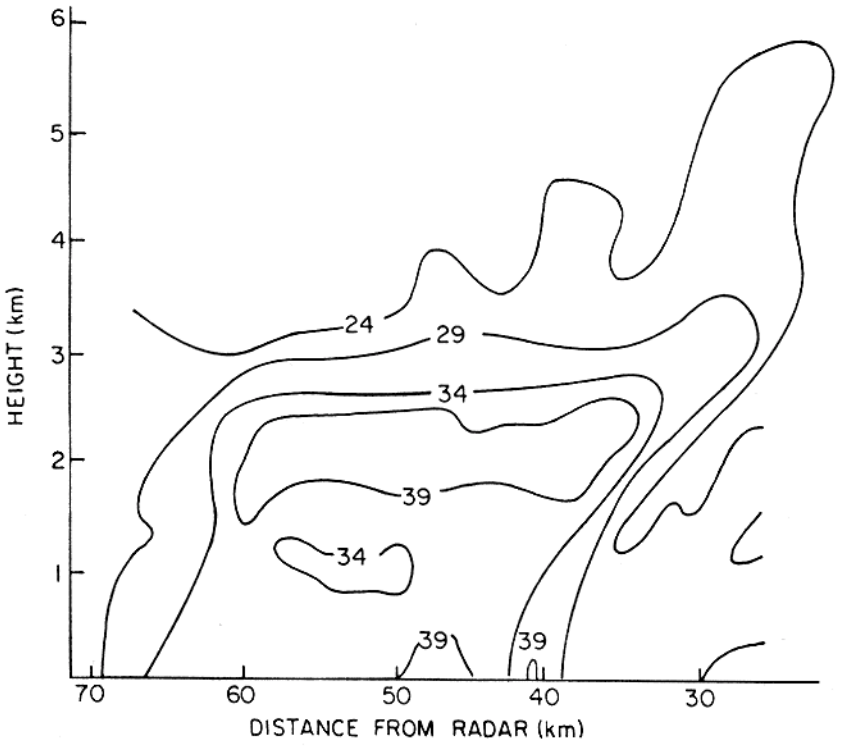

Fig. 1 Radar reflectivity pattern in the warm frontal rainband. The radar was located at Point Brown, Washington, and the data were taken along the 212° azimuth at 1130 LST 13 December 1977. Units are dBZ.

2. DATA

The air motions and radar reflectivity patterns associated with the rainband obtained in the CYCLES PROJECT with the NCAR* CP-3 Doppler Radar (Wavelength 5.45 cm, Peak Power 338 kW, Beam width 1°) which automatically collects, processes and records both the reflectivity and mean target velocity in 0.27 km data bins. This radar system was programmed for a sequence of scan modes at specified times including PPI, RHI and vertically pointing. Three-dimensional coverage was obtained at half-hour intervals by a sequence of conical scans.

Sounding data and other meteorological observations referred to in this study were obtained from the comprehensive set of data available from the CYCLES PROJECT observing systems (Hobbs et al., 1980).

3. METHOD OF AIR MOTION COMPUTATION

A two dimensional air motion pattern is derived from the Doppler velocity data by first selecting data from the azimuthal angle in the conical scan sequence that is perpendicular to the band. Let x be the horizontal coordinate normal to the band and z the height. The Doppler velocity data in the x-z plane were converted to values of the x-component u of the horizontal wind, and an isotach analysis was performed in the x-z plane. The velocity data were then transferred to a cartesian grid with horizontal spacing of 2.60 km and vertical spacing of 0.33 km. The horizontal divergence, $\Delta u/\Delta x$, was calculated for the entire field. A value of Δx of 5.2 km was used. It was assumed that the divergence of the horizontal wind along the band, or normal to the x-z plane, is small compared to $\Delta u/\Delta x$. Then, the continuity equation,

$$\frac{\Delta \omega}{\Delta p} = - \frac{\Delta u}{\Delta x} , \qquad (1)$$

where p is pressure and $\omega (\equiv dp/dt)$ is the vertical velocity, was integrated to obtain ω at 0.33 km intervals in the vertical. A lower boundary condition of no vertical motion is used, and p and z are used interchangeably assuming that they are related hydrostatically by $\delta p = - \rho g \, \delta z$, where g is the acceleration of gravity and ρ is the density given by $\rho_o \exp(-z/H)$, where ρ_o is the surface density and H is the scale height.

*National Center for Atmospheric Research

4. REFLECTIVITY PATTERN

The radar reflectivity pattern in the x-z plane is shown in Fig. 1. The rainband is well-defined with a pronounced melting layer indicated by the band of high reflectivity at approximately 2 km. The presence of the melting band suggests rather uniform conditions across the mesoscale precipitation feature at that altitude. Had convective-scale updrafts and downdrafts been present, the melting band would have been irregular or discontinuous. The irregular shape of the minimum detectable echo contour in Fig. 1, 30-50 km from the radar, probably indicates that weak convective cells were located aloft above the more stratiform lower layer, as is typical in warm frontal rainbands.

5. DIVERGENCE

The quantity $\Delta u/\Delta x$ computed from the Doppler velocity data is shown in the x-z plane in Fig. 2. To the extent that the rainband is two-dimensional this quantity is equal to the divergence of the horizontal wind. Fig. 2 and all subsequent figures involving air motion fields show values only within the boundary of the 34 dBZ echo contour. The Doppler velocities obtained near the boundary of the echo tended to be meteorologically unrealistic. To be cautious, we have, therefore, retained only the velocity measurements associated with echoes stronger than 30 dBZ in intensity.

At low levels (below 2 km), the values of $\Delta u/\Delta x$ were all in the range of -2×10^{-4} to -5×10^{-4} s^{-1}. This pattern extends continuously across the rainband, showing that the lower 2 km of the cloud associated with the rainband coincided with a mesoscale region of rather uniform convergence. Near the back edge of the rainband (60 km from the radar), the region of convergence extended upwards to the top of the echo. The middle of the upper portion of the echo is dominated by divergence of a magnitude similar to that of the convergence.

6. VERTICAL VELOCITY

The vertical velocity w throughout the rainband echo was upward, with magnitudes of tens of centimeters per second (Fig. 3). Vertical velocities of this magnitude are characteristic of mesoscale circulations, being an order of magnitude greater than synoptic-scale vertical velocities and one to two orders of magnitude less than convective updraft and downdraft speeds. The entire rainband below the 3 km level may, therefore, be regarded as a mesoscale upward motion feature. The double maximum in the pattern is apparently just a reflection of gradual undulations in the basic mesoscale pattern. They are not localized or intense enough to be considered embedded convective cells. As noted in discussing Fig. 1, weak convective cells may, however, have been located above the 3 km level.

7. AIRFLOW

The two dimensional airflow

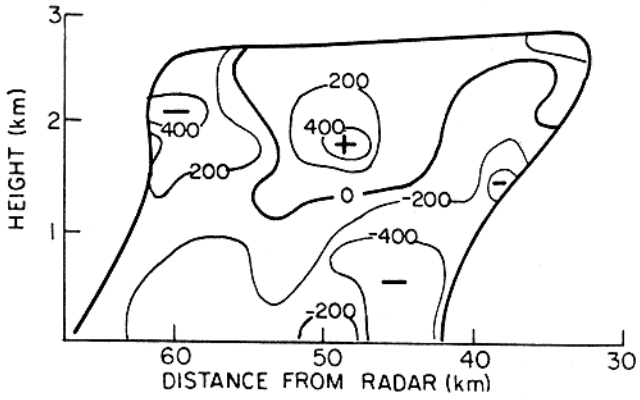

Fig. 2 Pattern of $\Delta u/\Delta x$ (in s^{-1}) in the warm frontal rainband echo. Outside boundary is 34 dBZ contour.

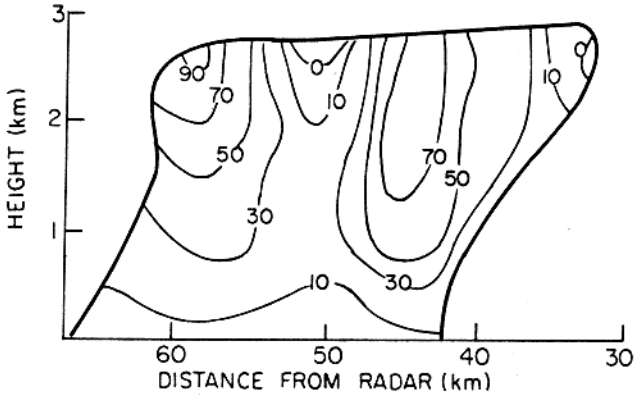

Fig. 3 Pattern of vertical velocity in the warm frontal rainband. Units are cm s^{-1}. Outside boundary is 34 dBZ contour.

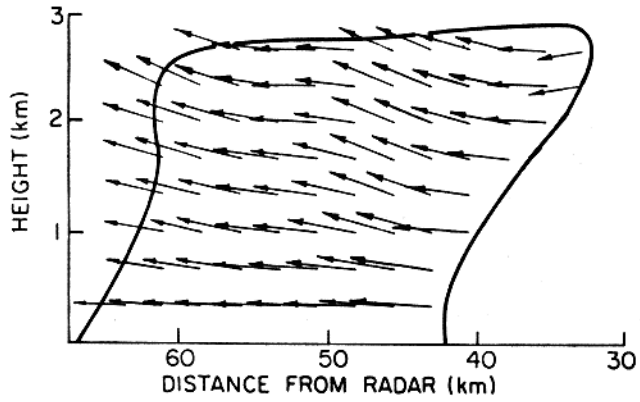

Fig. 4 Two-dimensional airflow relative to the rainband. Arrow shows 5 min displacement. Outside boundary is 34 dBZ contour.

relative to the rainband obtained by combining the measured horizontal component of the wind with the computed vertical velocity has a rather simple pattern (Fig. 4). Air flows in across the leading edge of the echo, rises slightly, then exits across the trailing boundary.

8. SURFACE PRESSURE

The region of enhanced vertical velocity and convergence associated with the rainband extended down into the planetary boundary layer (lowest 1 km). Convergence and vertical motion in the boundary layer are associated with cross-isobaric flow. Hence, a mesoscale perturbation in the surface pressure field may be expected to accompany the mesoscale perturbation in divergence and vertical velocity. The barograph trace obtained at the radar site during the passage of the rainband indeed shows such a perturbation. Mesoscale perturbations in pressure associated with rainbands are frequently noted in the CYCLES PROJECT; Houze et al. (1976b) identified and tracked several such features.

The vertical velocity associated with the pressure perturbation coinciding with the warm-frontal rainband in this study can be computed from Ekman layer theory (Holton 1972, p. 89) using the expression

$$w_E = \frac{D}{2\pi\rho f} \frac{\partial^2 p}{\partial x^2} \qquad (2)$$

where w_E is the vertical air velocity at the top of the Ekman layer, D is the depth of the Ekman layer, and f is the Coriolis parameter. From the barograph trace at the radar site, the value of $\partial^2 p/\partial x^2$ during the passage of the rainband was found to be between 2.2 and 2.9 mb km^{-2}. Assuming D = 1 km, ρ = 1.15 kg m^{-3} and f = 1.07 x 10^{-4} s^{-1}, we obtain values of w_E between 28 and 38 cm s^{-1}. These values are quite consistent with the values of w near the 1 km level in the rainband computed from (1) and shown in Fig. 3. Thus, the surface pressure field in the rainband is quantitatively consistent with the convergence and vertical velocities shown by the Doppler radar.

9. WATER BUDGET

The water budget of the rainband is examined by computing the condensation rate C within the volume V of the rainband. Assuming that the rainband was in a steady state and that no evaporation was occurring in the rainband, C is given by

$$C = -\iiint_V \nabla \cdot \rho q \vec{v}\, dV = \iint_S \rho q\, v_n\, dS, \qquad (3)$$

where $\vec{v}$ is the three-dimensional wind vector, q is the water vapor mixing ratio. S is the surface area of V, v_n is the inward directed component of $\vec{v}$ across S and Gauss' theorem has been used to obtain the third expression in (3). C was calculated with both the volume and the surface integrals.

The x-z face of the volume V used in the volume integral in (3) is a squared-off version of the 34 dBZ echo contour used to outline the rainband in previous figures (Fig. 5). This volume is presumed to extend indefinitely in a direction y normal to the x-z plane. We compute the condensate rate C in g s^{-1} for a unit length (1 cm) of the band in the y direction.

To evaluate the volume integral in (3), it is assumed that horizontal gradients of q are zero and that the air is saturated. Substitution of the continuity equation for steady state conditions,

$$\nabla \cdot \rho \vec{v} = 0, \qquad (4)$$

into (3) then leads to

$$C = -\iiint_V w\, \rho \frac{\partial q_s}{\partial z}\, dV \qquad (5)$$

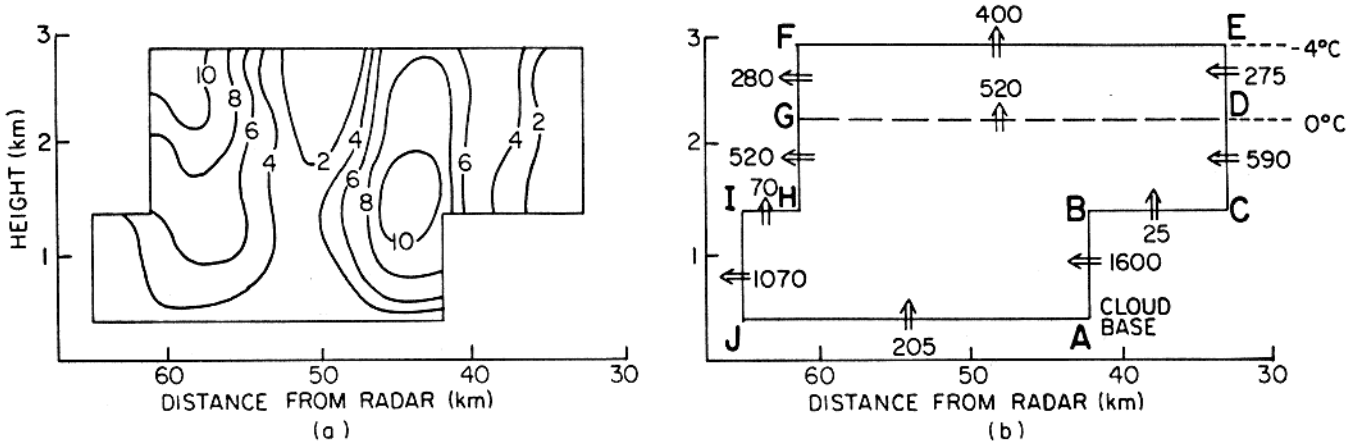

Fig. 5 (a) Condensation rate (in g s^{-1}) in the warm frontal rainband over a grid volume of 2.6 km x 0.3 km x 1 cm. (b) Vapor fluxes (in g s^{-1}) across boundaries of the rainband for a 1 cm length of the band normal to the cross section.

Table 1. *Condensation and precipitation rates for the rainband obtained by different methods. For precipitation, the average point value in the rainband is in mm h^{-1}, and the value obtained by applying this mean rate to the surface area covered by the rainband volume V defined in the text is given in g s^{-1}.*

CONDENSATION RATE BELOW THE -4°C LEVEL		
Volume Integral		400 g s^{-1}
Surface Integral		355
PRECIPITATION RATE IN THE RAINBAND		
Point Brown Gauge	8.2 mm h^{-1}	615 g s^{-1}
Moclips Gauge	4.9	365
Radar	7.8	580

where q_s is the saturation mixing ratio. The integrand is computed for individual volume elements (Δx = 2.6 km, Δz = 0.33 km, and Δy = 1 cm). The resulting field of condensation rate within V is shown in Fig. 5a. This field generally follows the field of w (Fig. 3), however, the centers of maximum condensation rate occur at lower levels than the centers of maximum w because of the strong decrease of the factor $\partial q_s/\partial z$ with height. The integrated condensation rate C obtained from the total volume integral (5) is 400 g $s^{-1}cm^{-1}$ (Table 1).

The contribution of the fluxes of water vapor across the various boundaries of V to the total condensation rate C, as computed by the surface integral in (3), is illustrated in Fig. 5b. The value of C obtained from the surface integral was 355 g s^{-1}, which agrees well with the value of 400 g s^{-1} obtained from the volume integral (Table 1). Almost all of the horizontal moisture convergence occurred in the lowest 1.4 km of the atmosphere. The net of the vapor fluxes across boundaries AB, AJ, JI, and IH was 655 g s^{-1}. The net of the fluxes across CD, BC and GH, by comparison, is only 95 g s^{-1} and that across DE and GH was -5 g s^{-1}.

Of the vapor converging into the rainband, 240 g s^{-1} was condensed below the 0°C level (Region ADGJ) and an additional 115 g s^{-1} was condensed in the layer between 0° and -4°C (Region DEFG). All of the condensation within the volume V took place below the -4°C level.

The condensation within V, as computed by both surface and volume integrals, is compared in Table 1 with measurements of the precipitation in the rainband. Four estimates of the precipitation rate are given. The Point Brown rain gauge, located at the radar site, and the Moclips gauge, 34 km north-northwest of the radar, registered rainfall rates differing by a factor of 0.6. These measurements sampled different parts of the band and were obtained 30 to 45 min after the radar measurements upon which the condensation calculations were based. It is difficult to say definitely which is more representative of the band at the time and location that it was sensed by the radar. However, subjectively, the band appeared on the radar to become less well organized as it approached Moclips, perhaps explaining the lower precipitation rate at that site and suggesting that the Point Brown measurement is more representative of the band in its well-defined stage. The precipitation rate in Table 1 calculated from the CP-3 radar data was obtained using the Z-R relationship of Marshall and Palmer (1948),

$$Z = 200\ R^{1.6}. \qquad (6)$$

Distrometer data obtained at the radar site during the CYCLES PROJECT field phase of November-December 1976 were consistent with this relation. However, the CP-3 radar reflectivity values were found to be 4.3 dBZ low when checked against raingauge data using (6) (Wilson, personnel communication). Consequently, we increased the recorded reflectivities by this amount before applying (6). The precipitation rate of 580 g s^{-1} thus obtained from the radar data in the rainband agrees well with the Point Brown raingauge, further suggesting that it gave a more representative reading than the Moclips gauge.

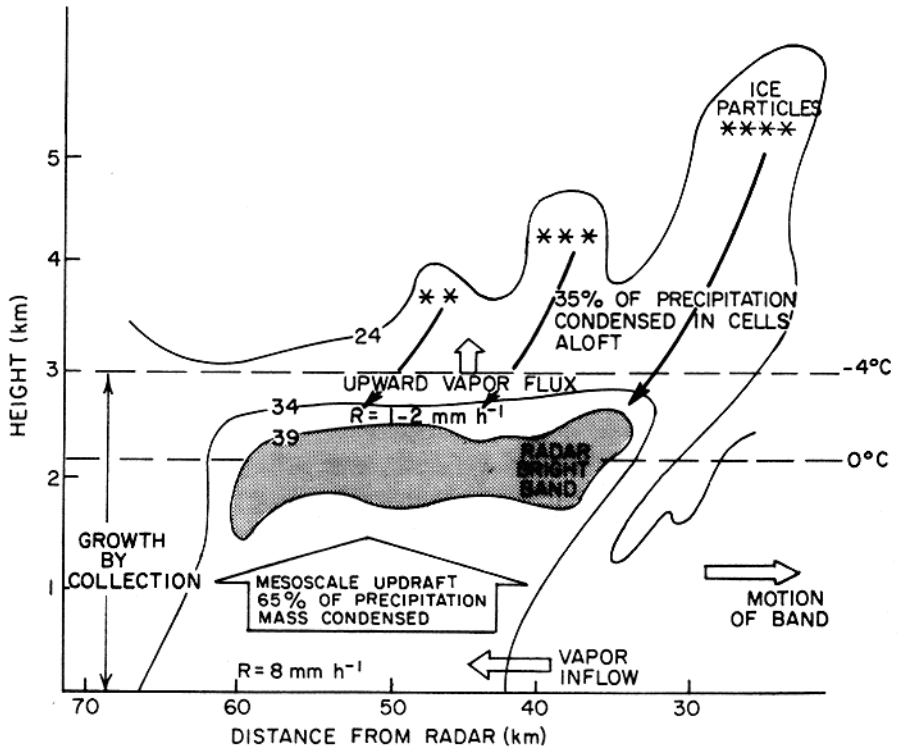

Fig. 6 Schematic illustration of the dynamical and microphysical precipitation processes associated with the warm frontal rainband. Radar echo contours are taken from Fig. 1.

Considering the Point Brown gauge and the radar rainfall measurement as the better indications of the rainfall rate of the rainbands, we conclude from Table 1 that the precipitation rate R was about 600 g s^{-1}, while the condensation rate C below the -4°C level was about 380 g s^{-1}. The remaining 220 g s^{-1} of the precipitation must be explained by condensation that occurred above the -4°C level. Much of this condensation probably occurred in the convective cells noted aloft in Fig. 1. The upward flux of water across the top boundary EF of the volume in Fig. 5b (400 g s^{-1}) more than adequately supplies the moisture for this condensation aloft. Thus, vapor convergence at low levels apparently supplies all the moisture necessary to account for the precipitation from the rainband, with 0.65 (= C/R) of the precipitation explained by condensation occurring in the stratiform low-level cloud and 0.35 (= 1 - C/R) explained by condensation in the layer of convective cells aloft.

10. CONCLUSIONS

The warm frontal rainband in this study was similar to the warm-feeder rainband of Herzegh and Hobbs (1980) in that it was characterized by a stratiform low-level radar echo with indications of convective cells located aloft. The stratiform layer was entirely below the -4°C level and was enhanced by non-convective, mesoscale lifting. Associated with the mesoscale lifting was water vapor convergence in the lowest 1.4 km of the atmosphere, which supplied all the moisture required to explain the surface precipitation of the rainband. The mesoscale lifting below the -4°C level led to the condensation of enough of the converged moisture to explain 65% of the precipitation. The remaining 35% of the precipitation was explained by condensation aloft of vapor converged at low levels but transported upward across the -4°C level by the mesoscale vertical motion. Above the -4°C level, this moisture was apparently concensed in convective cells overriding the stratiform echo region below. The connection of the lower layer to the upper layer by the upward flux of vapor indicates that the moisture convergence associated with the mesoscale updraft at low levels ultimately accounted for all of the precipitation in the rainband.

The condensation that occurred below the -4°C level and accounted for 65% of the precipitation was evidently condensed as liquid droplets in this layer. However, the horizontal wind relative to the rainband advecting these particles across the band al-

lowed $\lesssim$ 40 min for the particles to grow, which is probably an insufficient time for the particles to have reached precipitable sizes. Hence, ice particles generated in the layer of convective cells aloft and falling into the layer below the -4°C level was evidently crucial in converting the large amounts of condensed water at low levels to precipitation by collecting it. The pronounced radar bright band associated with the rainband indicates that a considerable number of ice particles were drifting down into the lower layer. Using the Z-R relationship for snow of Sekhon and Srivastava (1970), we find that the snowfall rates just above the melting level (corresponding to 30-40 dBZ) could have been no larger than 1-2 mm h^{-1}. Since surface rainfall rates were $\approx$8 mm h^{-1} (Table 1), it is evident that the accretion of cloud water by the precipitation particles below the -4°C level was indeed substantial.

To summarize, it appears that the basic dynamical feature responsible for the warm-frontal rainband was a low-level non-convective mesoscale upward motion feature which (1) supplied all the moisture required for precipitation, (2) condensed 65% of this moisture in a stratiform cloud below the -4°C level, (3) transported the necessary moisture to upper levels for the remaining 35% of the precipitation to be condensed in convective cells, which in turn, produced ice particles, that upon falling through the lower layer, grew by accretion of liquid water and thus converted the condensate produced by mesoscale lifting at low levels to precipitation. Much of this growth by accretion took place below the 0°C level. These processes are summarized schematically in Fig. 6.

The view of the precipitation processes in a warm frontal rainband that we have deduced from a quantitative study of the mesoscale water vapor budget of the rainband shows that non-convective mesoscale lifting did occur in this rainband, that it indeed was the essential dynamical feature of the rainbands, and that it occurred at low levels with boundary-layer convergence as a key element of its structure. We have further deduced aspects of the precipitation processes that appear to be necessary for consistency with the observed water budget. The processes we have thus diagnosed confirm those determined by Herzegh and Hobbs (1980) and Matejka et al. (1980) from airborne particle samples and vertical profiles of radar reflectivity in warm-frontal rainbands. The deductions of microphysical processes in these bands are, however, rather qualitative at this stage. In future work, we plan to use water continuity models with parameterized microphysics in the context of air motion patterns similar to those observed by Doppler radar to carry out more quantitative tests of the types of precipitation processes that occur in these mesoscale rainbands.

ACKNOWLEDGEMENTS

Thanks are due to all members of the University of Washington's Cloud Physics Group and to personnel from the National Center for Atmospheric Research's (NCAR) Atmospheric Technology Division for their valuable contributions to this study. The CYCLES PROJECT is supported by grant ATM77-01344 from the Experimental Meteorology and Weather Modification Profram, Division of Atmospheric Sciences, National Science Foundation (NSF), the Air Force Office of Scientific Research (Contract F49620-77-C-0057), the Environmental Research Laboratories of NOAA (Grants 04-7-023 and 44033), and the U. S. Army Research Office (DAAG 29-79-G-0005). The CP-3 radar was provided by NCAR, which is sponsored by NSF.

REFERENCES

Herzegh, P. H., and P. V. Hobbs, 1980: The mesoscale and microscale structure and organization of clouds and precipitation in mid-latitude cyclones. II: Warm-Frontal clouds. J. Atmos. Sci. (accepted for publication).

Hobbs, P. V., T. J. Matejka, P. H. Herzegh, J. D. Locatelli, and R. A. Houze, Jr., 1980: The mesoscale and microscale structure and organization of clouds and precipitation in mid-latitude cyclones. I: A case study of a cold front. J. Atmos. Sci. (accepted for publication).

_____, and J. D. Locatelli, 1978: Rainbands, precipitation cores and generating cells in a cyclonic storm. J. Atmos. Sci., 35, 230-241.

Holton, J. R., 1972: An Introduction to Dynamic Meteorology. Academic Press, New York, 319 pp.

Houze, R. A., Jr., P. V. Hobbs, K. R. Biswas and W. M. Davis, 1976a: Mesoscale rainbands in extratropical cyclones. Mon. Wea. Rev., 104, 868-878.

_____, J. D. Locatelli, and P. V. Hobbs, 1976b: Dynamics and cloud microphysics of rainbands in an occluded frontal system. J. Atmos. Sci., 33, 1921-1931.

Matejka, T. J., R. A. Houze, Jr., and P. V. Hobbs, 1980: Microphysics and dynamics of the clouds associated with mesoscale rainbands in extratropical cyclones. Quart. J. Roy. Meteor. Soc. (accepted for publication).

Marshall, J. S. , and W. McK. Palmer, 1948: The distribution of raindrops with size. J. Meteor., 5, 165-166.

Sekhon, R. S. and R. C. Srivastava, 1970: Snow size spectra and radar reflectivity. J. Atmos. Sci., 27, 299-307.